Miniature Multi-Ion Sensor Integrated With Artificial Neural Network

Yuncong Chen, Zheyuan Tang, Yunjiao Zhu, Michael J. Castellano, and Liang Dong, *Member, IEEE*

***Abstract*—Low-cost, accurate monitoring of macronutrient ions in soils, plants, and water is highly desired to improve fertilizer management for maximum profitability and minimum negative environmental impacts. Traditional ion-selective electrodes (ISEs) suffer from interference from non-target ions. This paper reports the integration of artificial neural networks (ANNs) and a miniature sensor containing an array of three ISE-based sensing elements to improve accuracy of the sensor in detecting and quantifying target nitrate (NO_3^-), phosphate ($H_2PO_4^-$), and potassium (K^+) ions in the environment. The sensor outputs of NO_3^-, $H_2PO_4^-$, and K^+ ion concentrations are used to train and optimize ANNs. The optimized neural networks are applied to classify and estimate concentrations of the target ions in the presence of interfering ions. The ANN-assisted array of sensing elements reduces cross-sensitivity between these elements. The present sensor is validated with measurements of NO_3^-, $H_2PO_4^-$, and K^+ ions in soil solution, plant sap, and tile drainage water from crop fields.**

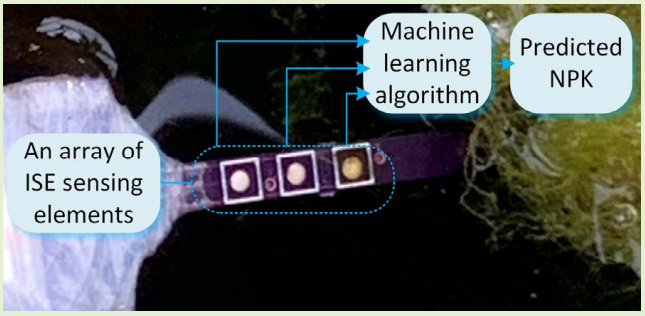

***Index Terms*—Agricultural sensor, ion-selective electrode, soil, plant, tile drainage water, ANN, cross sensitivity, machine learning.**

I. Introduction

NITROGEN phosphorus, and potassium are primary macronutrients essential for plant growth and development. Fertilizer application supplies crops with these nutrients. Under-application of fertilizer causes economic loss due to reduced grain yield and quality, while over-application causes economic loss due to unused fertilizer. Moreover, the unused fertilizer is typically lost to the environment, where it pollutes air and water resources. Crop production is the leading cause of nutrient losses to aquatic ecosystems [1], [2]. Regionally, nitrogen and phosphorus fertilizers are the leading cause of eutrophication and hypoxia in aquatic ecosystems, which promotes algal blooms and reduces biodiversity. Locally, nitrogen fertilizers pollute drinking water supplies; the maximum contaminant level (MCL) for nitrate ions in public water supplies is 10 mg N L^{-1} set by the United States Environmental Protection Agency [3]. High nitrate levels in drinking waters have been associated with a variety of negative human health outcomes. The recommended MCL of total phosphate in water streams to prevent eutrophication is 0.05 mg P L^{-1} [4]. Although potassium movement in soil is relatively slow and potassium fertilizers do not contribute to air and water pollution, potassium deficiency can reduce crop yield and quality, while potassium over-application has a detrimental effect on crop quality and soil productivity [5]. To reduce the fertilizer input costs and minimize their adverse environmental and human health effects, there is a need for improving our ability to accurately monitor nutrient status, fertilizer application, and environmental impact at low cost, which is of great benefit to agricultural producers and environmental conservation practitioners [6].

Laboratory-based ion measurement methods, such as ion chromatography, spectrophotometry, and chemoluminescence, offer high sensitivity and selectivity; but, these technologies are not suitable for field application due to high cost and bulky size [7], [8]. Portable spectrophotometers are an attractive solution to environmental monitoring of ions for agricultural management [9]; however, they are still relatively expensive and often require site-specific calibrations

Manuscript received August 10, 2021; revised September 30, 2021; accepted September 30, 2021. Date of publication October 4, 2021; date of current version November 12, 2021. This work was supported in part by the U.S. Department of Energy-Advanced Research Projects Agency-Energy (DOE-ARPA-E) under Award DE-AR0000824; in part by the U.S. Department of Agriculture-National Institute of Food and Agriculture (USDA-NIFA) under Grant 2018-67021-27845, Grant 2020-67021-31528, and Grant 2020-68013-30934; in part by the U.S. National Science Foundation under Grant CNS-2125484; and in part by the Plant Sciences Institute, Iowa State University. The associate editor coordinating the review of this article and approving it for publication was Prof. Mahesh Kumar. *(Corresponding author: Liang Dong.)*

Yuncong Chen, Zheyuan Tang, and Liang Dong are with the Department of Electrical and Computer Engineering, Iowa State University, Ames, IA 50011 USA (e-mail: ldong@iastate.edu).

Yunjiao Zhu and Michael J. Castellano are with the Agronomy Department, Iowa State University, Ames, IA 50011 USA.

Digital Object Identifier 10.1109/JSEN.2021.3117573

for field applications. Many miniaturized nutrient ion sensors and measurement systems have been reported based on different sensing mechanisms [10], such as ion-selective electrode (ISE) [11], ion-selective field-effect transistor [12], [13], microwave resonance [14], [15], colorimetry [16], fiber-optic spectroscopy [17], electrochemical measurement [18], [19], microfluidic electrophoresis chips [20], and enzymatic sensing [21], [22]. But, much room exists to improve the sensitivity, selectivity, stability, and cost-efficiency of these miniaturized ion sensors. For example, permeable biocatalytic membranes have also been integrated into microfluidic sensors to facilitate ion movement into measurement chambers where enzymes are used to reduce specific ions for quantification [24], [25] but their selectivity and sensitivity are compromised by the instability of enzyme molecules used in the sensors.

ISE-based sensors are widely used in analytical chemistry due to their simple structure and low cost. But, these sensors suffer from a signal drift and instability over time because there is an issue with chloride leaching from silver/silver chloride (Ag/AgCl)-based pseudo reference electrodes (REs) due to the redox reaction occurring at these REs [26]. Also, ion-selective membranes (ISM) of the ISEs are interfered with by non-target ions. The ion exchange-induced potential E at the ISE is described as $E = \text{constant} + (R \times T / z \times F) \times ln\ [\alpha + \sum_i (k_i\ \alpha_i^{z/zi})]$, where R is the gas constant, T is the temperature, F is the Faraday constant, z and z_i are the charge of the target ion and interfering ion i, respectively, α is the chemical activity for the relevant ion, and k_i represents the selectivity coefficient [27]. It should be noted that because the potential E is logarithmic to the sum of the total activities of both target and non-target ions, ISEs exhibit a non-optimal ion selectivity under the exposure to various ion species in environments; this makes ISEs not a popular solution to detection of nutrient ions in agricultural soil solution and plant sap where dissolved ions are extremely rich. In addition, a thin water layer often develops and is trapped at the interface between the ISM and the conducting base electrode of the ISE. This thin water layer acts as not only as a barrier to the transfer of electrons to the base electrode but also a trap that catches all kinds of ions, thus affecting the selectivity of ISEs [28]. Although the above-mentioned issues can be alleviated to some extent by innovating ISE materials and structures, such as coating a protection layer on the surface of Ag/AgCl REs and introducing a solid-state ion-to-electron transducing layer below the ISM [29]–[33], there is still room to improve the selectivity of the ISE-based sensors.

Recently, machine learning has proven a promising solution for improving the measurement accuracy of various sensors. Supervised learning are often used to perform classification and regression using datasets from multiple interconnected sources, where the training input data and their target outputs are available and the algorithms can make predictions on the input data set and use the given true value for improving the prediction [34]. Unsupervised learning algorithms are used to determine the distribution of data set in the input space or to find a set of similar examples in the input data set [34]. Because supervised and unsupervised learning has the ability to interrogate nonlinear dependencies for complex systems, considerable efforts have been made to use machine learning techniques for interpretation of sensing data, discrimination of complex signals, and prediction of target analytes. For example, semi-supervised machine learning alleviated a drifting issue in a dynamic pattern recognition framework by adapting a regressor or classifier as unlabeled samples [35]. Principal component analysis allowed for feature extraction and target classification by reducing signal dimensions to only a primary component [36]. Deep neural network algorithms assisted in extracting hidden signals below a limit-of-detection level in gas sensing [37]. Continuum-removal algorithms helped to estimate nitrogen concentration from aircraft-acquired hyperspectral data for plant leaves [38]. Gaussian processes were used to assess chlorophyll content, nitrogen content, and leaf water content from a field-based multi-species dataset [39]. Backpropagation neural network algorithms made it possible to characterize wine properties with the help of a bionic electronic nose [40]. Artificial neural network (ANN) algorithms were adopted to enhance the selectivity of a potentiometric tongue sensor to sulfide and perchlorate anions [41].

This paper presents the incorporation of ANN algorithms with a multi-ion sensor to reduce cross-sensitivity between multiple sensing elements of the sensor for improving accuracy in measuring nitrate (NO_3^-), phosphate ($H_2PO_4^-$), and potassium (K^+) ions in agricultural soil solution, plant sap, and tile drainage water. An array of three ISE-based sensing elements is formed on one side of a printed circuit board (PCB). Each ISE element is coated with an ISM that ideally can target a specific NO_3^-, $H_2PO_4^-$, or K^+ ion (Fig. 1a and 1b). On the other side of the PCB is an Ag/AgCl-based RE. The sensor is shaped to a needle that can help to insert into the stalk of plants for in-situ measurement of target ions, while for ion sensing in soil solution and tile drainage water, the needle shape is not required. An ANN model is constructed to reduce the cross-sensitivity of the three ISEs through modeling the relationship between the input and output data of the neural network (Fig. 1c). The ANN is trained using the responses of the three ISEs to prepare mixed-ion solutions with known NO_3^-, $H_2PO_4^-$ and K^+ concentrations. Key parameters of the ANN are optimized to improve performance in predicting NO_3^-, $H_2PO_4^-$ and K^+ ion concentrations. Prediction performance of the ANN is evaluated by root mean squared error (RMSE) and coefficient of determination (R^2). The three ISE-based sensing elements have different sensing characteristics and can probe differential interactions with ion species. The ANN analyzes these interactions and learns a model based on a part of the data to perform data classification and regression. The present multi-ion sensor, in conjunction with the optimal ANN, is demonstrated to identify and quantify NO_3^-, $H_2PO_4^-$ and K^+ ions in different samples obtained from agriculture cropland.

II. Experimental

A. Materials

NO_3^- ISM cocktail was prepared by mixing methyltriphenylphosphonium bromide (0.25 wt %), nitrocellulose (moistened with 2-propanol (35%); 1.93 wt %), 2-nitrophenyl

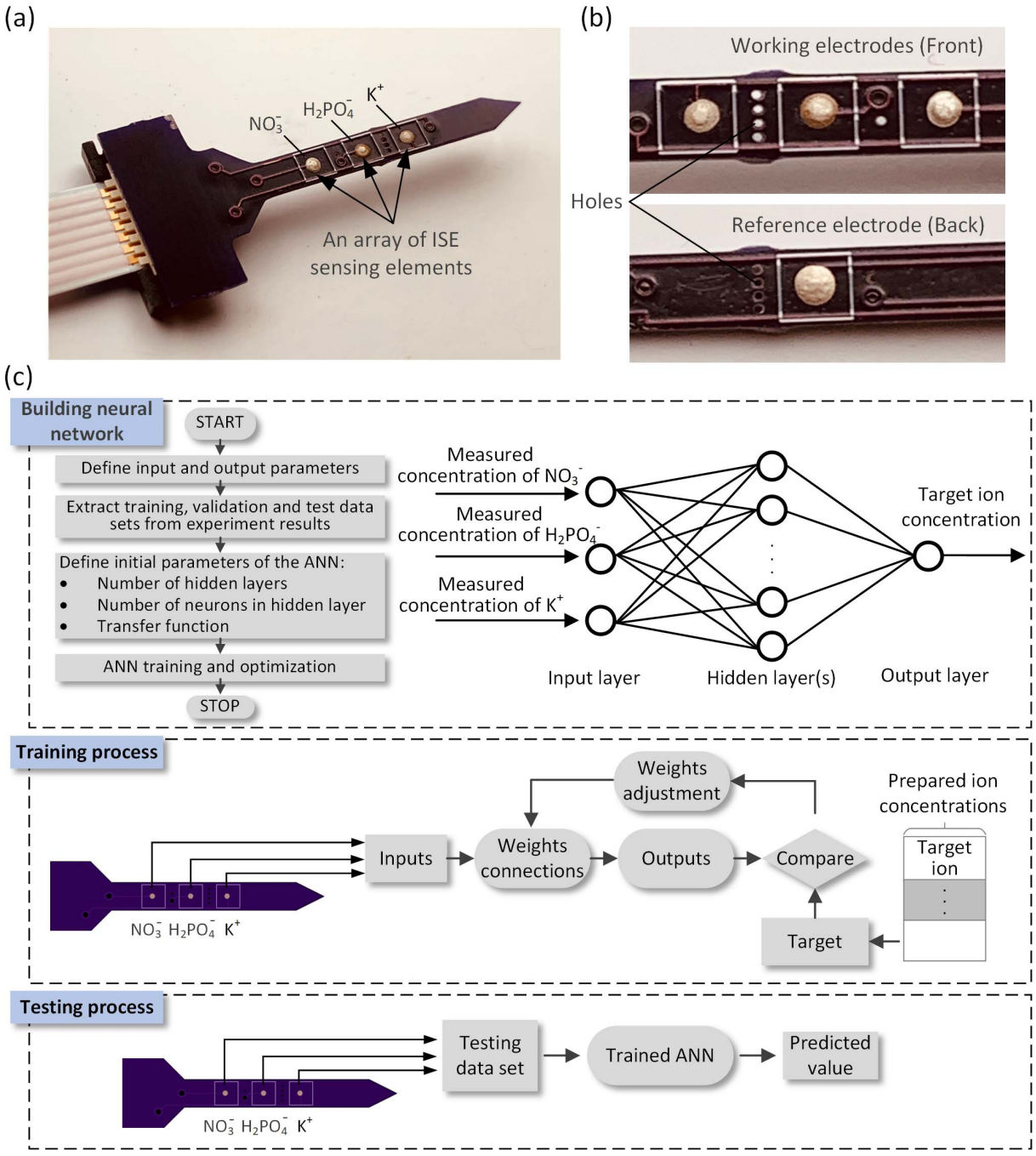

Fig. 1. (a) and (b) Photos of the fabricated multi-ion sensor containing an array of three ISE-based sensing elements to detect NO_3^-, $H_2PO_4^-$ and K^+ ions. (a) These sensing elements are formed on one side of a needle-shaped PCB. (b) An Ag/AgCl-based RE is shared by the three sensing elements and formed on the other side of the PCB. (c) Diagrams of building, training, and testing ANNs for improving accuracy in estimating concentrations of NO_3^-, $H_2PO_4^-$ and K^+ ions.

octyl ether (NPOE) (16.25 wt %), polyvinyl chloride (PVC) (5.75 wt %), tetrahydrofuran (THF) (74.3 wt %), and tridodecylmethylammonium nitrate (1.50 wt %). $H_2PO_4^-$ ISM cocktail was prepared by mixing tributyltin chloride (0.1 wt %), NPOE (6.55 wt %), PVC (3.27 wt %), and sodium tetrakis-[3,5- bis(trifluoromethyl)phenyl]borate (NaTFPB) (0.07 wt %) and THF (90 wt %). K^+ ISM cocktail was formed with valinomycin (0.2 wt %), PVC (6.56 wt %), NPOE (13.2 wt %), potassium tetrakis-[3,5- bis(trifluoromethyl)phenyl]borate (KTFPB) (0.04 wt %), and THF (80 wt %). These cocktail solutions were stirred using a magnetic stirrer for 12 hours and stored at -20 °C. Single-salt standard ion solutions were prepared by dissolving appropriate amounts of $NaNO_3$, NaH_2PO_4, or KCl in deionized (DI) water. For each ion type (NO_3^-, $H_2PO_4^-$ or K^+), four concentrations (10^{-4} M, 10^{-3} M, 10^{-2} M and 10^{-1} M) were also prepared.

A set of 63 training samples was prepared and used to train ANN models, consisting of a mixture of NO_3^-, $H_2PO_4^-$ and K^+ ions with the concentration of each ion type varying among

0, 10^{-4} M, 10^{-3} M, and 10^{-2} M. In addition, the other set of 126 samples with two interfering ions (Cl^- and Ca^{2+} ions) was prepared by adding 10^{-3} M NaCl alone, or both 10^{-3} M NaCl and 10^{-4} M $CaCl_2$ together into the above-mentioned 63 training samples. Here, Cl^- and Ca^{2+} ions were selected as interfering ions because Cl^- ions can significantly affect the stability of Ag/AgCl-based RE, and Ca^{2+} is one of the critical cations present in soils and plants [42].

B. Device Fabrication

The multi-ion sensor was manufactured on a 0.8 mm-thick PCB (OSH PARK) that had a needle shape. The needle part of the sensor was 25 mm-long and 4.2 mm-wide. The three ISEs of the sensor shared a single RE placed on the other side of the PCB. The RE was formed by screen-printing 0.2 mm thick, 1 mm diameter Ag/AgCl ink on a 0.8 mm-diameter circular copper contact pad with the help of a stencil mask, and then was dried on a hotplate at 110 °C for 2 hours. Similarly, to form the ISEs, three circular copper contact pads (0.8 mm diameter each) were coated with 0.2 mm thick, 1 mm diameter Ag/AgCl ink using the screen-printing method; next, the corresponding ISM solutions of NO_3^-, $H_2PO_4^-$ and K^+ were drop casted on the surface of the Ag/AgCl electrodes and dried at room temperature for 10 hours. The multiple through-holes were created on the PCB to allow exposing all the ISEs and RE to the same medium, thus forming a closed circuit to perform the potentiometric measurement.

C. Testing Setup

To calibrate the ISEs, each ISE was preconditioned by immersing into a standard NO_3^-, $H_2PO_4^-$ or K^+ ion solution with 10^{-1} M ion concentration for 24 hours. After cleaning with DI water, the ISE was immersed into a single-salt standard solution of target ion with a known concentration for 3 minutes, and then the voltage output from the ISE was recorded once every second using a homemade data logger. After the testing, the ISE was cleaned with DI water again to remove residual ions from the surface of ISE. The calibration for each ISE was performed with a series of concentrations of the target ion from low to high, and from high to low, and then from low to high. Therefore, each ion concentration was measured by the ISE in triplicate. Fig. 2 shows the potentiometric output of each ISE as a function of concentration of the target ion. Also, the sequence of triplicate measurements indicates no hysteresis in the measurement data.

Next, the calibrated sensor with the three ISEs was utilized to measure NO_3^-, $H_2PO_4^-$ and K^+ ion concentrations of the 63 training samples with no interfering ions and of the 126 samples containing Cl^- and Ca^{2+} interfering ions. Specifically, the sensor readings of the training samples were utilized for training and optimizing ANN models while the sensor readings of the samples with the interfering ions were employed to validate the ability of the optimized ANN in reducing the influence of the interfering ions on the estimation accuracy of the sensor.

TABLE I
PARAMETERS OF THE ANN MODELS

Parameters	Values	Definitions
Hidden layer size	8, 10, 15, 20	# of neurons in a hidden layer
Max. # hidden layers	3	# of hidden layers
Adaptive value μ	0.001, 0.1	Controlling magnitude of weight changes based on output errors
μinc	1.5, 10	Increase factor of μ
μdec	0.1, 0.5	Decrease factor of μ
Training goal	10^{-8}	Goal for RMSE to stop training
Max. # of epochs	10,000	Training stops if full set of the data greater than this number of times
Hidden layer transfer function	tansig	Hyperbolic tangent sigmoid transfer function that calculates hidden layer's output from net input
Output layer transfer function	purelin	Linear transfer function for output calculation
Training fraction	0.7	Training subset data fraction
Validation fraction	0.15	Validation subset data fraction
Testing fraction	0.15	Testing subset data fraction

D. Optimization of ANN Architecture

Two types of ANN models were constructed. The first type (namely, individual ANN model) was built to predict a single ion species of NO_3^-, $H_2PO_4^-$ or K^+, while the other type (namely, group ANN model) intended to predict all three ion species together. Each model utilized the sensor-measured concentrations of the three ions as the inputs of the model. Training of the ANN model was conducted using the Neural Network Toolbox in Matlab. The full set of the training data was split into three subsets: training (70% of the training data), validation (15%), and testing (15%). Table I gives the values of each parameter of the ANN model tested in the simulation. The ANN models were then ranked based on the RMSE and R^2 values between the prepared and the ANN-predicted ion concentrations. Lower RMSE and higher R^2 values indicate a better prediction performance of the model.

III. RESULTS AND DISCUSSION

Table II summarizes the performance of the individual and group ANN models for predicting NO_3^-, $H_2PO_4^-$ and K^+ ions in the absence of interfering ions. As indicated by the lower RMSE and higher R^2 values, the individual ANN model exhibits a higher accuracy in predicting a single ion species than the group ANN model does to predict the three different ions together as a group.

Next, the optimal individual ANN models (Table II) were used to predict the concentration of NO_3^-, $H_2PO_4^-$, and K^+ ions present in the prepared training samples without interfering ions. The scatter plots in Fig. 3a-3c show the sensor-measured concentrations and the ANN-predicted outputs with respect to the prepared ion concentrations of the training samples. The red line with the slope of 1.0 in each data plot shows the perfect correlation between the prepared ion concentration and the measured and predicted ion concentration. The ANN predictions give smaller RMSE values than the sensor readings. Specifically, for the determination of NO_3-, H_2PO_4- and K+ ions, the individual ANN models reduce the RMSE values from 0.53, 1.50, and 1.73 to 0.28, 0.31, and

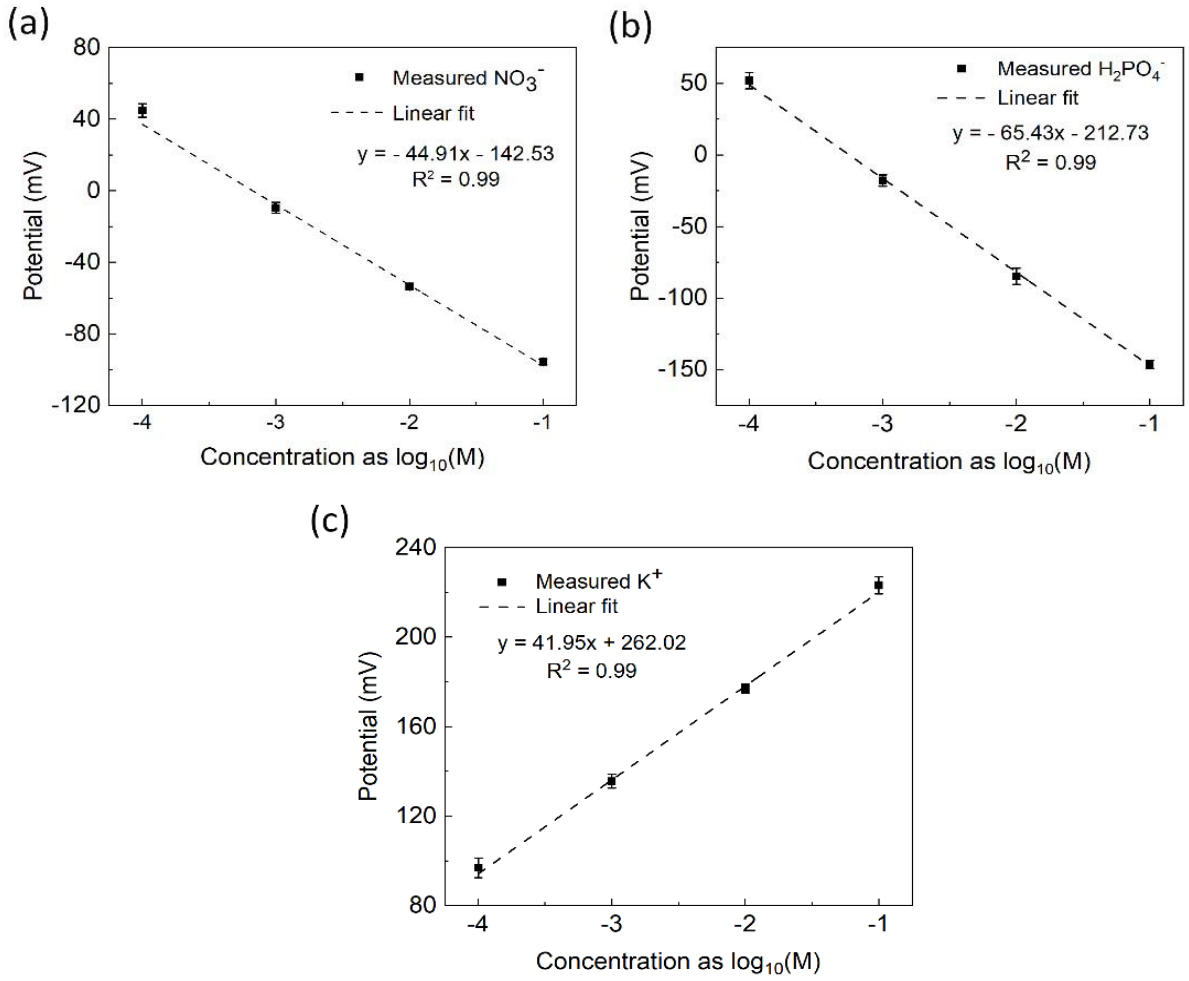

Fig. 2. Calibration curves of the ISEs, showing the output voltage of each ISE as a function of concentration of target ion: **(a)** NO_3^-, **(b)** $H_2PO_4^-$, and **(c)** K^+. The calibration was performed with a series of ion concentrations in single-salt solutions.

TABLE II
PARAMETERS OF THE OPTIMAL ANNS FOR PREDICTING NO_3^-, $H_2PO_4^-$ AND K^+ ION CONCENTRATIONS IN THE ABSENCE OF INTERFERING IONS

Type of ion	# of neurons in hidden layer 1	# of neurons in hidden layer 2	# of neurons in hidden layer 3	RMSE	R2
Individual ANN model					
NO3-	15	0	0	0.28	96%
H2PO4-	8	8	0	0.31	96%
K+	8	15	0	0.30	96%
Group ANN model					
NO3-, H2PO4- and K+	15	10	8	0.58	82%

0.30, respectively. The slopes of the linear fitting curves for the ANN-predicted NO_3-, H_2PO_4- and K+ ion concentrations are 0.934, 0.927, and 0.943, respectively, indicating a considerable correlation of the predicted ion concentrations to the prepared ones.

Further, the optimal individual ANNs were used to predict the concentrations of NO_3-, H_2PO_4- and K+ ions in the samples containing not only NO_3-, H_2PO_4- and K+ ions, but also Cl^- and Ca^{2+} interfering ions. The prepared concentrations of NO_3-, H_2PO_4- and K+ ions were set as the targets of the output layer of each individual ANN, while the sensor-measured concentrations were set as the three inputs of the input layer of the ANN. The Cl^- and Ca^{2+} ion concentrations were treated as the unknown input values for the ANN. The scatter plots in Fig. 4a-4c show that, for measuring the concentrations of NO_3-, H_2PO_4- and K+ ions, the sensor measurements provide the RMSE values of 0.48, 0.55, and 0.66, respectively; while the ANN models result in the RMSE values of 0.35, 0.46, and 0.43 with the slopes of the linear fitting curves at 0.968, 0.889, and 0.925, respectively. Therefore, for a given target ion, the ANN prediction exhibits a smaller RMSE value than the sensor measurement, indicating that the incorporation

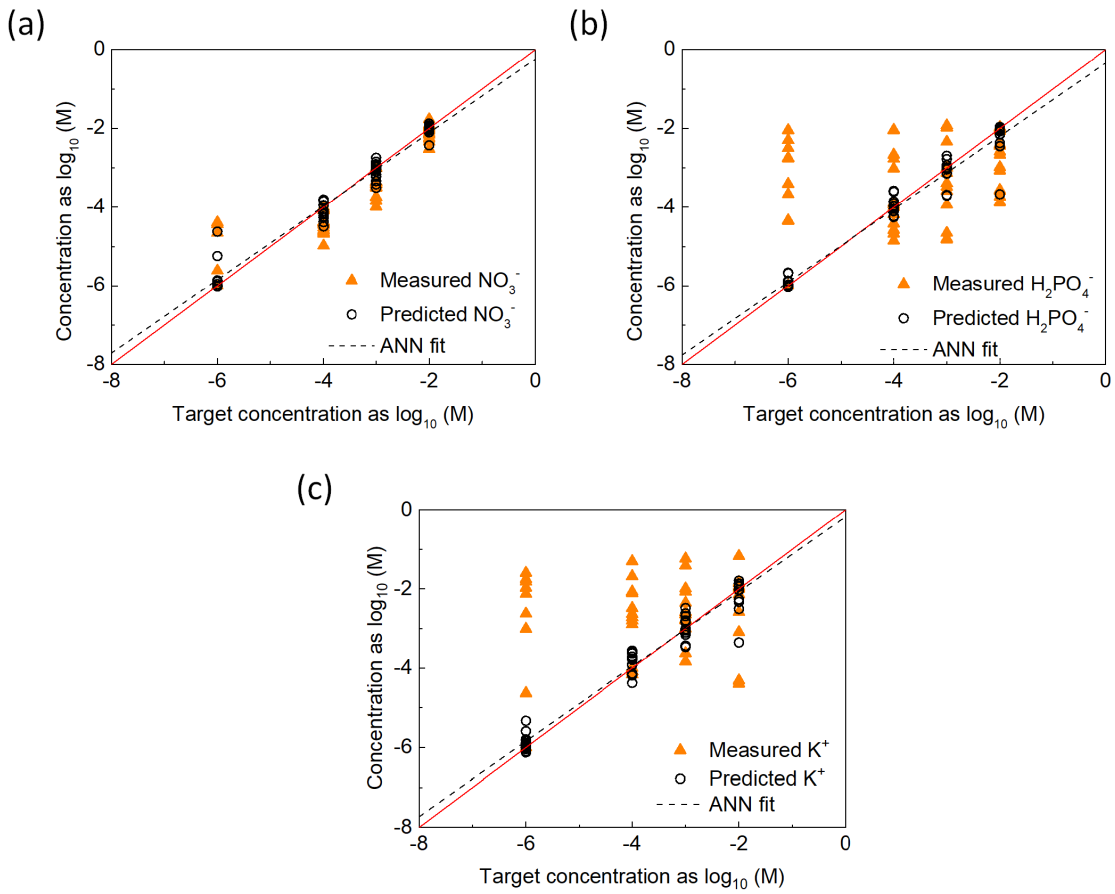

Fig. 3. Scatter data plots showing the ion concentrations of **(a)** NO_3-, **(b)** H_2PO_4-, and **(c)** K+ measured by the sensor and predicted by the optimal individual ANNs (Y-axis) with respect to the prepared ion concentrations (X-axis) in training-samples without interfering ions.

TABLE III
PARAMETERS OF THE OPTIMAL INDIVIDUAL ANNS FOR PREDICTING NO_3^-, $H_2PO_4^-$ AND K^+ ION CONCENTRATIONS IN THE PRESENCE OF CL^- AND CA^{2+} INTERFERING IONS

Type of ion	# of neurons in hidden layer 1	# of neurons in hidden layer 2	RMSE	R^2
NO_3^-	20	0	0.35	94%
$H_2PO_4^-$	8	10	0.46	95%
K^+	8	15	0.43	95%

of the ANN model on the sensor measurement data can improve the measurement accuracy even in the presence of interfering ions. Table III summarizes the ANN settings and the obtained RMSE and R^2 values for predicting NO_3^-, $H_2PO_4^-$ and K^+ ion concentrations in the presence of Cl^- and Ca^{2+} ions. The RMSE values become higher, and the R^2 values become lower with Cl^- and Ca^{2+} ions, compared to those obtained with no interfering ions (Table II).

Moreover, the incorporation of the ANN model with the three-element sensor improved the accuracy in determining NO_3^-, $H_2PO_4^-$ and K^+ ion concentrations in various real samples from agriculture croplands, maize stalk sap, soil solution, and drainage (i.e., 'tile') water. For in-situ measurement of NO_3^-, $H_2PO_4^-$ and K^+ ions in maize stalks, plants (genotype: B73) were grown in the greenhouse. The sensor measurement was conducted at the V8 growth stage [43]. The sensor was directly inserted into the stalk at ~8 cm above the soil surface. The sensor was then left in the stalk until the signal became stable. Next, the sensor was used to measure NO_3^-, $H_2PO_4^-$ and K^+ ions in soil solution. The soil was placed on a cellulose filter paper (Whatman) in a funnel and became water saturated by adding 500 ml water that contained NO_3^-, $H_2PO_4^-$ and K^+ ions of 10^{-3} M concentration each. To validate the machine learning-assisted sensor in measuring NO_3^-, $H_2PO_4^-$ and K^+ ions in agricultural tile drainage water, water samples were collected from drainage systems on the Iowa State University research farm (Ames, Iowa). The sensor was dipped into the collected sample for direct measurement. For comparison, we also performed traditional measurements of NO_3^-, $H_2PO_4^-$ and K^+ ions in the fluids squeezed from the stalk at the insertion location of the needle sensor, the drained water from the soil-containing funnel, and the collected tile drainage water. The traditional measurements included inductively coupled plasma mass spectrometry (ICP-MS; PlasmaQuantMS Elite, Analytik Jena) for $H_2PO_4^-$ and K^+ ions and liquid chromatography (LC; 1260 Infinity II System, Agilent Technologies) for NO_3^- ion in these samples.

Fig. 5 shows the results of the sensor-measured, analytical instruments-measured, and individual ANN-predicted NO_3^-, $H_2PO_4^-$ and K^+ ion concentrations in the stalk, soil, and

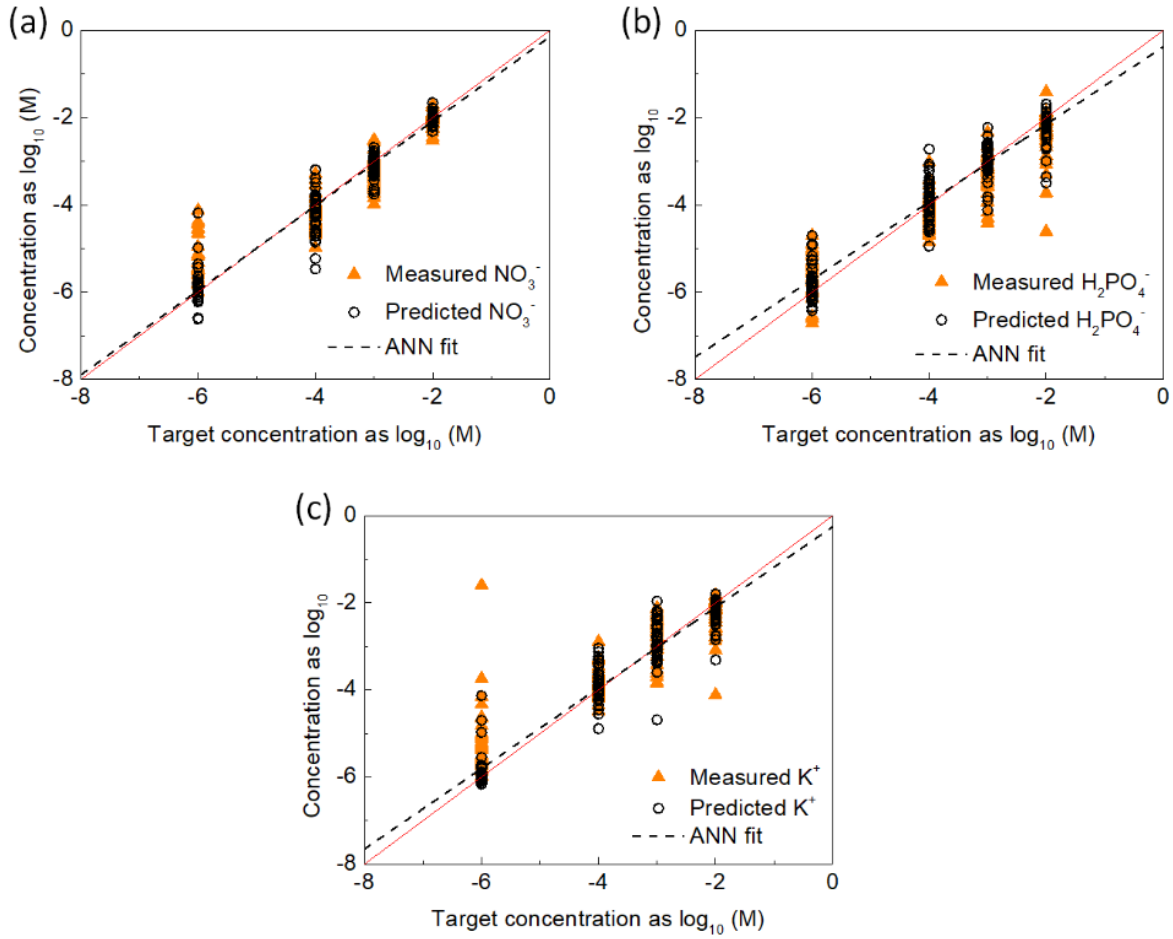

Fig. 4. Scatter data plots showing the ion concentrations of **(a)** NO_3-, **(b)** H_2PO_4-, and **(c)** K+ measured by the sensor and predicted by the optimal individual ANNs (Y-axis) with respect to the prepared ion concentrations (X-axis) in training-samples that contained the Cl- and Ca2+ interfering ions.

tile drainage water samples. The result indicates that the individual ANN model can improve the measurement accuracy over the direct sensor measurement. For NO_3^-, $H_2PO_4^-$ and K^+ ions, the RMSE values with the sensor alone were found to be 0.68, 4.85, and 0.90, respectively; however, the ANN-assisted estimation helped lower the RMSE values to 0.28, 0.69, and 0.70, respectively. Also, for NO_3^-, $H_2PO_4^-$, and K^+ ions, the R^2 values of the ANN-predicted result were 92%, 71%, and 81%, respectively, while the R^2 values with the sensor alone increased to 71%, 59%, and 79%, respectively. Therefore, compared to the sensor alone, the incorporation of the ANN with the sensor improved the measurement accuracy substantially for NO_3^- and $H_2PO_4^-$ ions (Fig. 5a-5b), but only slightly for K^+ ion. The difference in the efficacy of the ANN model for predicting the three ion species may be associated with the difference of the ISEs in selecting the corresponding target ions. As shown in Fig. 5c, the sensor-measured data for K^+ ions appeared more disperse than those for NO_3^- and $H_2PO_4^-$ ions, indicating the lower selectivity of the ISM for K^+ ion compared to the other two ISMs for NO_3^- and $H_2PO_4^-$ ions.

The present sensor includes three ISE-based sensing elements with different sensing characteristics. These elements exhibit differential interactions with analytes. These readings from these elements are analyzed by the machine learning algorithm to detect and quantify target ions. There is much room to improve the accuracy of the ANN-assisted sensor for estimating different ion species in environments. Numerous ion species exist in real samples and interfere measurement accuracy of the sensor. The bias in the determination of the target ion species is affected by these interfering ions but can be reduced by increasing the number of the ISE-based sensing elements, where each ISE uses an ISM responsible for a target ion ideally. Also, by increasing the data set size of the calibration for the sensor, it is possible to improve the prediction accuracy of the neural network. We believe that by improving the selectivity of each sensing element to its target species, the response diversity across multiple sensing elements of the device will be increased, which, in turn, will aid in discrimination and quantification for the target species from the background interferences in the environment. Other future efforts include expanding the detection capability of the present sensor system from NO_3^-, $H_2PO_4^-$, and K^+ to not only other agriculturally important nutrient ions such as NO_2^-, SO_4^{2-}, NH_4^+, Cl^-, Mg^{2+}, Ca^{2+} and Na^+, but also physical parameters such as temperature, moisture, and water

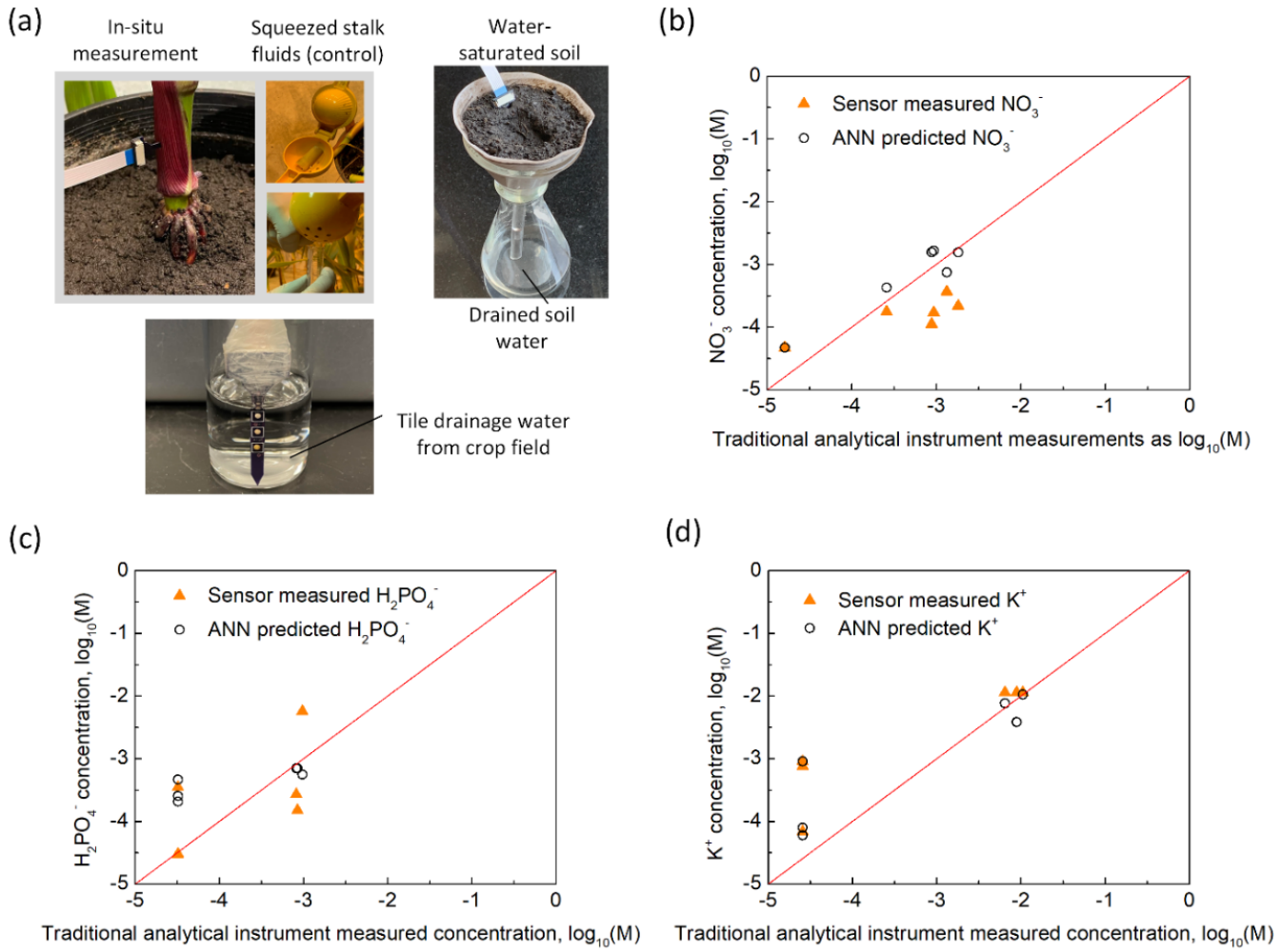

Fig. 5. Photos of the sensor for measuring NO_3^-, $H_2PO_4^-$, and K^+ ions in different samples. Upper left: the sensor was inserted into the stalk of a maize plant; upper right: the sensor was placed in the soil; lower: the sensor was placed in the tile drainage water collected from the crop field. The traditional analytical instruments were used to test the following samples, including the squeezed fluids from the stalk using a juice squeezer (upper middle), the drained water from the soil in the funnel (upper right), and the same tile drainage water collected from the farm. Scatter data plots show the concentrations of **(b)** NO_3-, **(c)** H_2PO_4-, and **(d)** K+ ions measured using the sensor and predicted using the ANN (Y-axis) with respect to the results obtained using the traditional analytical instrument (X-axis).

potential [44]. From an application perspective, in addition to improving fertilizer management [45], the machine learning-assisted array of sensing elements can be modified to detect many other biochemical compounds of environmental concern such as pesticides [46], volatiles [47], and greenhouse gas emissions (e.g., nitrous oxide, carbon dioxide, and methane).

IV. Conclusion

A machine learning-assisted multi-ion sensor was developed to improve the identification and quantification of NO_3^-, $H_2PO_4^-$ and K^+ ions in various samples in agriculture. The ANN model was optimized to reduce cross-sensitivities between the three ISE-based sensing elements integrated on the sensor. The prediction for a single ion species by an individual ANN was more accurate than the prediction for all three ions together using a single ANN. Three optimized individual ANNs were used to estimate the concentrations of NO_3^-, $H_2PO_4^-$, and K^+ ions, respectively; the result shows that they provided the prediction accuracy of 96% across the three ions based on the R^2 value that examined the linearity between the predicted and actual ion concentrations. Further, the ANN-assisted multi-ion sensing approach exhibited an improved ability to measure the target ions in the presence of interfering ions. Lastly, this method was validated in detecting these nutrient ions in the stalk, soil, and tile drainage water in agriculture.

Acknowledgment

The authors would like to thank Dr. Patrick Schnable, Dr. Baskar Ganapathysubramanian, Hussam Ibrahim, Koushik Nagasubramanian, and Raufur Rahman Khan for insightful discussions.

References

[1] M. B. David, L. E. Drinkwater, and G. F. McIsaac, "Sources of nitrate yields in the Mississippi River basin," *J. Environ. Qual.*, vol. 39, no. 5, pp. 1657–1667, Sep. 2010.

[2] R. B. Alexander, R. A. Smith, G. E. Schwarz, E. W. Boyer, J. V. Nolan, and J. W. Brakebill, "Differences in phosphorus and nitrogen delivery to the Gulf of Mexico from the Mississippi River basin," *Environ. Sci. Technol.*, vol. 42, no. 3, pp. 822–830, Feb. 2008.

[3] *National Primary Drinking Water Regulations*, Standard EPA 816-F-09-004, United States Environmental Protection Agency, 2009.

[4] D. W. Litke, "Review of phosphorus control measures in the United States and their effects on water quality: US geological survey water-resources investigations report 99-4007," US Geol. Surv. Fact Sheet, Columbia, SC, USA, Tech. Rep. S-007-98, 1999.

[5] F. Zhang *et al.*, "Potassium nutrition of crops under varied regimes of nitrogen supply," *Plant Soil*, vol. 335, nos. 1–2, pp. 21–34, Oct. 2010.

[6] M. A. Ali, L. Dong, J. Dhau, A. Khosla, and A. Kaushik, "Perspective—Electrochemical sensors for soil quality assessment," *J. Electrochem. Soc.*, vol. 167, no. 3, Jan. 2020, Art. no. 037550.

[7] O. H. Ahmed, G. Sumalatha, and A. M. N. Muhamad, "Use of zeolite in maize *(Zea mays)* cultivation on nitrogen, potassium and phosphorus uptake and use efficiency," *Int. J. Phys. Sci.*, vol. 5, no. 15, pp. 2393–2401, 2010.

[8] O. J. Idowu *et al.*, "Farmer-oriented assessment of soil quality using field, laboratory, and VNIR spectroscopy methods," *Plant Soil*, vol. 307, nos. 1–2, pp. 243–253, Jun. 2008.

[9] R. A. V. Rossel, D. J. J. Walvoort, A. B. McBratney, L. J. Janik, and J. O. Skjemstad, "Visible, near infrared, mid infrared or combined diffuse reflectance spectroscopy for simultaneous assessment of various soil properties," *Geoderma*, vol. 131, nos. 1–2, pp. 59–75, Mar. 2006.

[10] C. Dimkpa, P. Bindraban, J. E. McLean, L. Gatere, U. Singh, and D. Hellums, "Methods for rapid testing of plant and soil nutrients," in *Sustainable Agriculture Reviews*. Cham, Switzerland: Springer, 2017, pp. 1–43.

[11] R. Rosenberg, M. S. Bono, S. Braganza, C. Vaishnav, R. Karnik, and A. J. Hart, "In-field determination of soil ion content using a handheld device and screen-printed solid-state ion-selective electrodes," *PLoS ONE*, vol. 13, no. 9, Sep. 2018, Art. no. e0203862.

[12] J. Artigas *et al.*, "Application of ion sensitive field effect transistor based sensors to soil analysis," *Comput. Electron. Agricult.*, vol. 31, no. 3, pp. 281–293, May 2001.

[13] Y. Jiao *et al.*, "In-planta nitrate detection using insertable plant microsensor," in *Proc. 20th Int. Conf. Solid-State Sens., Actuator Microsyst. Eurosensors XXXIII*, 2019, pp. 37–40.

[14] R. V. Rossel, V. I. Adamchuk, K. A. Sudduth, N. J. McKenzie, and C. Lobsey, "Proximal soil sensing: An effective approach for soil measurements in space and time," *Adv. Agron.*, vol. 113, pp. 243–291, Jan. 2011.

[15] S. Roy, N. M. Neihart, and N. Bowler, "Coaxial microwave resonant sensor design for monitoring ionic concentration in aqueous solutions," in *Proc. IEEE Int. Instrum. Meas. Technol. Conf. (I2MTC)*, May 2018, pp. 1–6.

[16] R.-T. Liu *et al.*, "A miniaturized on-chip colorimeter for detecting NPK elements," *Sensors*, vol. 16, no. 8, p. 1234, Aug. 2016.

[17] F. Monteiro-Silva, P. A. S. Jorge, and R. C. Martins, "Optical sensing of nitrogen, phosphorus and potassium: A spectrophotometrical approach toward smart nutrient deployment," *Chemosensors*, vol. 7, no. 4, p. 51, Oct. 2019.

[18] M. A. Ali *et al.*, "Tunable bioelectrodes with wrinkled-ridged graphene oxide surfaces for electrochemical nitrate sensors," *RSC Adv.*, vol. 6, pp. 67184–67195, Jul. 2016.

[19] L. Burton, K. Jayachandran, and S. Bhansali, "The 'real-time' revolution for *in situ* soil nutrient sensing," *J. Electrochem. Soc.*, vol. 167, no. 3, 2020, Art. no. 037569.

[20] Z. Xu, X. Wang, R. J. Weber, R. Kumar, and L. Dong, "Nutrient sensing using chip scale electrophoresis and *in situ* soil solution extraction," *IEEE Sensors J.*, vol. 17, no. 14, pp. 4330–4339, Jul. 2017.

[21] M. A. Ali *et al.*, "*In situ* integration of graphene foam–titanium nitride based bio-scaffolds and microfluidic structures for soil nutrient sensors," *Lab Chip*, vol. 17, no. 2, pp. 274–285, 2017.

[22] M. A. Ali *et al.*, "Microfluidic impedimetric sensor for soil nitrate detection using graphene oxide and conductive nanofibers enabled sensing interface," *Sens. Actuators B, Chem.*, vol. 239, pp. 1289–1299, Feb. 2017.

[23] H. Ibrahim, S. Moru, and L. Dong, "A biochemical sensor with artificial 3D enzyme network," in *Proc. IEEE 33rd Int. Conf. Micro Electro Mech. Syst. (MEMS)*, Jan. 2020, pp. 697–700.

[24] W. Xuejiang *et al.*, "Conductometric nitrate biosensor based on methyl viologen/nafion/nitrate reductase interdigitated electrodes," *Talanta*, vol. 69, no. 2, pp. 450–455, Apr. 2006.

[25] P. Si and E. Bakker, "Thin layer electrochemical extraction of non-redoxactive cations with an anion-exchanging conducting polymer overlaid with a selective membrane," *Chem. Commun.*, vol. 35, pp. 5260–5262, Oct. 2009.

[26] J. Bobacka, "Potential stability of all-solid-state ion-selective electrodes using conducting polymers as ion-to-electron transducers," *Anal. Chem.*, vol. 71, no. 21, pp. 4932–4937, Oct. 1999.

[27] J. Bobacka, A. Ivaska, and A. Lewenstam, "Potentiometric ion sensors," *Chem. Rev.*, vol. 108, pp. 329–351, Jan. 2008.

[28] A. Cadogan, Z. Gao, A. Lewenstam, A. Ivaska, and D. Diamond, "All-solid-state sodium-selective electrode based on a calixarene ionophore in a poly(vinyl chloride) membrane with a polypyrrole solid contact," *Anal. Chem.*, vol. 64, no. 21, pp. 2496–2501, Nov. 1992.

[29] J. Bobacka, M. McCarrick, A. Lewenstam, and A. Ivaska, "All solid-state poly(vinyl chloride) membrane ion-selective electrodes with poly(3-octylthiophene) solid internal contact," *Analyst*, vol. 119, no. 9, pp. 1985–1991, 1994.

[30] K. Y. Chumbimuni-Torres, N. Rubinova, A. Radu, L. T. Kubota, and E. Bakker, "Solid contact potentiometric sensors for trace level measurements," *Anal. Chem.*, vol. 78, no. 4, pp. 1318–1322, Feb. 2006.

[31] N. Rubinova, K. Chumbimunitorres, and E. Bakker, "Solid-contact potentiometric polymer membrane microelectrodes for the detection of silver ions at the femtomole level," *Sens. Actuators B, Chem.*, vol. 121, no. 1, pp. 135–141, Jan. 2007.

[32] M. A. Ali *et al.*, "Continuous monitoring of soil nitrate using a miniature sensor with poly(3-octyl-thiophene) and molybdenum disulfide nanocomposite," *ACS Appl. Mater. Interfaces*, vol. 11, no. 32, pp. 29195–29206, 2019.

[33] Y. Zhu *et al.*, "Continuous *in situ* soil nitrate sensors: The importance of high-resolution measurements across time and a comparison with salt extraction-based methods," *Soil Sci. Soc. Amer. J.*, vol. 85, no. 3, pp. 677–690, 2021.

[34] F. Cui, Y. Yue, Y. Zhang, Z. Zhang, and H. S. Zhou, "Advancing biosensors with machine learning," *ACS Sensors*, vol. 5, no. 11, pp. 3346–3364, Nov. 2020.

[35] S. De Vito, G. Fattoruso, M. Pardo, F. Tortorella, and G. Di Francia, "Semi-supervised learning techniques in artificial olfaction: A novel approach to classification problems and drift counteraction," *IEEE Sensors J.*, vol. 12, no. 11, pp. 3215–3224, Nov. 2012.

[36] M. Penza, G. Cassano, and F. Tortorella, "Gas recognition by activated WO_3 thin-film sensors array," *Sens. Actuators B, Chem.*, vol. 81, no. 1, pp. 115–121, Dec. 2001.

[37] S.-Y. Cho *et al.*, "Finding hidden signals in chemical sensors using deep learning," *Anal. Chem.*, vol. 92, no. 9, pp. 6529–6537, May 2020.

[38] Z. Huang, B. J. Turner, S. J. Dury, I. R. Wallis, and W. J. Foley, "Estimating foliage nitrogen concentration from HYMAP data using continuum removal analysis," *Remote Sens. Environ.*, vol. 93, nos. 1–2, pp. 18–29, Oct. 2004.

[39] S. Van Wittenberghe, J. Verrelst, J. P. Rivera, L. Alonso, J. Moreno, and R. Samson, "Gaussian processes retrieval of leaf parameters from a multi-species reflectance, absorbance and fluorescence dataset," *J. Photochem. Photobiol. B, Biol.*, vol. 134, pp. 37–48, May 2014.

[40] H. Liu, Q. Li, B. Yan, L. Zhang, and Y. Gu, "Bionic electronic nose based on MOS sensors array and machine learning algorithms used for wine properties detection," *Sensors*, vol. 19, no. 1, p. 45, Dec. 2018.

[41] D. Wilson, M. N. Abbas, A. L. A. Radwan, and M. D. Valle, "Potentiometric electronic tongue to resolve mixtures of sulfide and perchlorate anions," *Sensors*, vol. 11, no. 3, pp. 3214–3226, Mar. 2011.

[42] F. C. Steward, Ed., *Plant Physiology 9: A Treatise: Water and Solutes in Plants*. vol. 9. Amsterdam, The Netherlands: Elsevier, 2012.

[43] L. J. Abendroth, R. W. Elmore, M. J. Boyer, and S. K. Marlay, "Corn growth and development," Dept. Agronomy, Iowa State Univ. Extension Publication, Ames, IA, USA, Tech. Rep. PMR-1009, 2011. [Online]. Available: https://store.extension.iastate.edu/product/Corn-Growth-and-Development

[44] Y. Chen, Y. Tian, X. Wang, L. Wei, and L. Dong, "Miniaturized, field-deployable, continuous soil water potential sensor," *IEEE Sensors J.*, vol. 20, no. 23, pp. 14109–14117, Dec. 2020.

[45] P. Zhang, Z. Guo, S. Ullah, G. Melagraki, A. Afantitis, and I. Lynch, "Nanotechnology and artificial intelligence to enable sustainable and precision agriculture," *Nature Plants*, vol. 7, no. 7, pp. 864–876, Jul. 2021.

[46] R. Umapathi *et al.*, "Colorimetric based on-site sensing strategies for the rapid detection of pesticides in agricultural foods: New horizons, perspectives, and challenges," *Coordination Chem. Rev.*, vol. 446, no. 1, 2021, Art. no. 214061.

[47] Z. Li *et al.*, "Non-invasive plant disease diagnostics enabled by smartphone-based fingerprinting of leaf volatiles," *Nature Plants*, vol. 5, no. 8, pp. 856–866, Aug. 2019.

Yuncong Chen received the B.S., M.S., and Ph.D. degrees from Iowa State University in 2015, 2017, and 2021, respectively, all in electrical engineering. His research interest includes low-cost and miniature sensors for environmental monitoring.

Zheyuan Tang received the B.S. and M.S. degrees in electrical engineering from Iowa State University in 2019 and 2021, respectively.

Yunjiao Zhu received the B.S. degree in agricultural water conservancy engineering from Hohai University, China, in 2018. She is currently pursuing the Ph.D. degree in soil sciences with the Agronomy Department, Iowa State University.

Michael J. Castellano received the Ph.D. degree in soil science from The Pennsylvania State University in 2009. He is the William T. Frankenberger Professor of Soil Science with the Agronomy Department, Iowa State University. His research focuses on maximizing sustainable productivity of crop systems. He has particular interest in nitrogen because nitrogen is a costly input and often limits crop production, but is easily lost to the environment where it becomes an economic loss that degrades air and water quality.

Liang Dong (Member, IEEE) received the Ph.D. degree in electronic science and technology from the Institute of Microelectronics, Tsinghua University, China, in 2004. From 2004 to 2007, he was a Postdoctoral Research Associate with the University of Wisconsin-Madison. He is the Vikram L. Dalal Professor with the Department of Electrical and Computer Engineering, Iowa State University. His research interests include MEMS, sensors, micro-fluidics, micro-optics, and advanced materials and manufacturing and their applications in agriculture, environment, plant and animal science, and biomedicine. He serves as the Editor-in-Chief of *Sensors and Actuators A: Physical*, an Associate Editor for *Micro & Nano Letters*, and a Topic Editor for *Biosensors*.